



# CHORUS

This is the accepted manuscript made available via CHORUS. The article has been published as:

## Theoretical optical and x-ray spectra of liquid and solid $H_{2}O$

J. Vinson, J. J. Kas, F. D. Vila, J. J. Rehr, and E. L. Shirley  
Phys. Rev. B **85**, 045101 — Published 3 January 2012

DOI: [10.1103/PhysRevB.85.045101](https://doi.org/10.1103/PhysRevB.85.045101)

# Theoretical optical and x-ray spectra of liquid and solid H<sub>2</sub>O

J. Vinson,<sup>1</sup> J. J. Kas,<sup>1</sup> F. D. Vila,<sup>1</sup> J. J. Rehr,<sup>1</sup> and E. L. Shirley<sup>2</sup>

<sup>1</sup>*Dept. of Physics, Univ. of Washington Seattle, WA 98195*

<sup>2</sup>*National Institute of Standards and Technology, Gaithersburg, MD 20899*

(Dated: December 13, 2011)

Theoretical optical and x-ray spectra of model structures of water and ice are calculated using a many-body perturbation theory, Bethe-Salpeter equation (BSE), approach implemented in the valence- and core-excitation codes AI2NBSE and OCEAN. These codes use *ab initio* density-functional theory wave functions from a plane-wave, pseudopotential code, quasi-particle self-energy corrections, and a BSE treatment of particle-hole interactions. This approach improves upon independent-particle methods through the inclusion of a complex, energy-dependent self-energy and screened particle-hole interactions to account for inelastic losses and excitonic effects. These many-body effects are found to be crucial for quantitative calculations of ice and water spectra.

PACS numbers: 71.15Qe, 61.05.cj, 61.25.Em

## I. INTRODUCTION

Recently there has been considerable interest and controversy surrounding the connection between the local structure of water and ice and their observed optical and x-ray spectra.<sup>1–16</sup> Part of the difficulty lies in modeling the structures of these complex, finite-temperature systems. Conventional super-cell methods require large unit cells to treat proton-disorder in ice and a configurational average adequate to represent a statistical ensemble of water structures. Structural probes such as x-ray and neutron scattering do not provide an unambiguous interpretation of the local geometry.<sup>17</sup> Another part of the difficulty lies in theoretical modeling. Despite many attempts, quantitative theoretical calculations of the optical and x-ray spectra of these systems have proved to be notoriously difficult due to strong non-local, self-energy, and excitonic effects. Thus the various theoretical methods that have been employed to date exhibit considerable variation in their results, undermining a definitive interpretation.<sup>6,8,14–16,18</sup>

In an effort to address these issues, we present calculations of the valence and core excitation spectra of well-characterized model ice and water systems based on a recently developed approach utilizing the Bethe-Salpeter equation (BSE) and Hedin's GW approximation for the quasi-particle self-energy (the acronym GW refers to the product of the one-electron Green's function  $G$  and the screened Coulomb interaction  $W$ ),<sup>19</sup> within a pseudopotential plane-wave basis. This GW/BSE approach has been implemented in the AI2NBSE and OCEAN packages for valence and core-level spectra respectively.<sup>20,21</sup> The method is advantageous compared to independent-electron approximations,<sup>3,5,6,8,12,16,18</sup> in that it provides a first-principles method for the inclusion of both quasi-particle and excitonic effects. These many-body effects modify peak positions, widths, and strengths, and hence they are crucial for a quantitative treatment and interpretation of the spectra. GW/BSE calculations have been carried out previously for both the valence<sup>22,23</sup> and core<sup>15</sup> spectra of water, with various approximations

for the screened particle-hole interaction. A key difference is that our implementation uses a complex, energy-dependent GW self-energy, in addition to screening the core-hole potential within the random phase approximation.

The remainder of this paper is as follows: The theoretical methods are summarized in Sec. II. Results for two forms of ice are presented in Sec. III and for a model water system in Sec. IV. Finally, Sec. V contains a summary and suggestions for further work.

## II. THEORETICAL METHODS

### A. GW/BSE Approach

The theory behind the GW/BSE approach implemented in AI2NBSE and OCEAN for valence and core excitations is described in detail in Refs. 20 and 21 respectively, so only a short summary is included here. The BSE represents the equation of motion of a particle-hole state, here an electron photo-excited into the conduction bands from either the occupied valence bands (optical) or a deep oxygen  $1s$  orbital (x-ray). Briefly, the open-source plane-wave, pseudopotential code ABINIT<sup>24,25</sup> is used to calculate both occupied and unoccupied Kohn-Sham density functional theory (DFT) states of the ground-state Hamiltonian, which serve as a basis for the BSE. This Kohn-Sham calculation uses the Ceperley-Alder, Perdew-Wang local density approximation for the exchange-correlation potential.<sup>26</sup> DFT orbitals only strictly describe a non-interacting system, but they can be good approximations to quasi-particle wavefunctions and perturbatively corrected, e.g., via Hedin's GW approximation. In this work, first-order quasi-particle energy corrections are added through the GW many-pole self-energy (MPSE) approximation of Kas et al.<sup>27</sup> In contrast to previous GW/BSE approaches for these systems,<sup>22,23</sup> our MPSE is complex and energy-dependent, and thus accounts for both the energy shifts and inelastic losses which stretch and damp the spectral

features. This MPSE model is based on a many-pole fit to AI2NBSE calculations of the valence loss spectrum  $-\text{Im} \epsilon^{-1}(\omega)$ .

The optical and x-ray spectra, the latter including both x-ray absorption (XAS) and non-resonant inelastic x-ray scattering (NRIXS), which is also referred to as x-ray Raman spectra (XRS), are then calculated using the National Institute of Standards and Technology (NIST) BSE solver in AI2NBSE<sup>20</sup> and OCEAN<sup>21</sup> respectively. The core spectra in OCEAN use atomic core-level states and projector-augmented-wave (PAW) transition matrix elements.<sup>28</sup> The BSE kernel includes both a screened direct attraction between the electron and hole and an unscreened, repulsive exchange term. The treatment of the particle-hole interactions is an important consideration due to the weakly screened excitonic effects in water and ice. In both our valence and core codes the screened Coulomb interaction  $W$  is approximated as statically screened. A Hybertsen-Levine-Louie dielectric function is implemented in AI2NBSE, while OCEAN uses the random-phase approximation (RPA) at short-range, switching to a model dielectric function at long range.<sup>29,30</sup> It should be noted that the radius governing the cross-over from RPA to model dielectric function is adjustable, and convergence of the screening has been tested, ensuring that the screening is equivalent to an RPA calculation at both short and long range. In contrast, previous approaches have relied on a variety of approximations based on self-consistent screening with DFT.<sup>2,3,5,6,12-16</sup>

In a disordered system like liquid water, the core  $1s$  states of each oxygen are subject to a different static potential and to slightly different screening by the valence electrons, resulting in shifts in the energy of the core hole.<sup>31</sup> Exact absolute energies are not calculated with our pseudopotential based method, but relative shifts were determined according to the relation

$$E_{1s} = E_{1s}^{av} + V^{\text{KS}} + (1/2)W_C. \quad (1)$$

$E_{1s}^{av}$  is the site-independent binding energy which is taken to be dependent on the pseudopotential and aligned to match experiment. The second term  $V^{\text{KS}}$  is the total Kohn-Sham potential at the site, including the effects of all the other ionic cores. The last term is the effect of the spectator electrons screening the core hole, reducing the energy necessary to excite the  $1s$  electron. Both  $V^{\text{KS}}$  and  $W_C$  are evaluated at the oxygen site. These binding-energy shifts lead to a slight broadening of the liquid water spectra in Fig. 7. For both ice-Ih (Fig. 4) and water (Fig. 7) an  $E_{1s}^{av}$  value of 401.4 eV results in good agreement with experiment, but for ice-VIII (Fig. 5) an additional 0.9 eV shift is necessary.

## B. Structures

The pair distribution function (PDF)  $g(R)$  and total electronic density of states (DOS) provide useful mea-

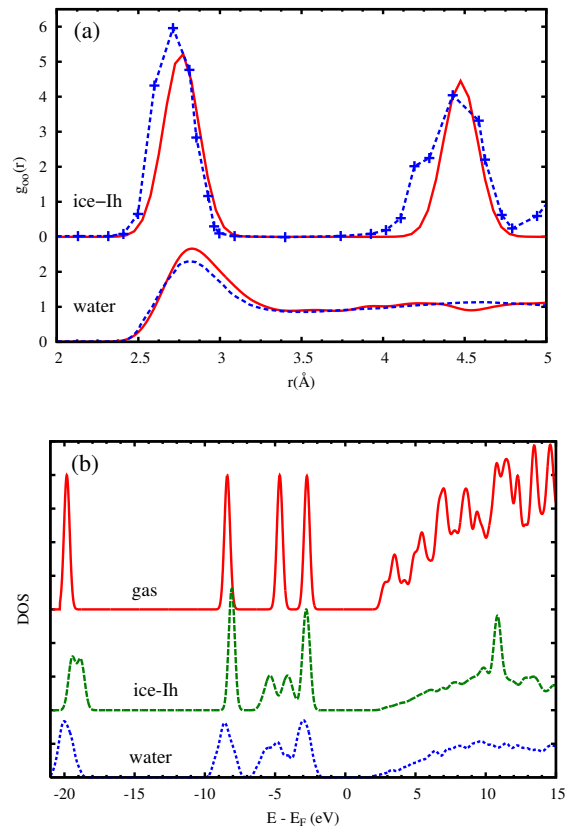


FIG. 1: (Color online) a) The oxygen-oxygen pair distribution function,  $g_{OO}(R)$ , for our model structure unit cells (red, solid line) compared with experimental results for ice<sup>32</sup> (blue plusses) and water data from Narten et al. analyzed by Soper<sup>33</sup> (blue, dotted line); b) comparison of the total electronic density of states for ice-Ih, liquid water, and gas-phase models, calculated using ABINIT. The broadening and vertical scaling are the same for all three structures, and energies are relative to the Fermi level. The features for the liquid cell are naturally broadened by structural disorder.

asures of the ground-state structural and electronic properties of our model ice and water systems (Fig. 1). In order to interpret x-ray and optical spectra, it is important that the model structures used in the calculations match observed structural properties, e.g., the PDF from neutron or x-ray diffraction. For our model ice-Ih cell  $g_{OO}(R)$  is in reasonable agreement with experiment. However, the first shell peak is shifted to a slightly larger mean radius. To be consistent with experiment a root-mean-square disorder of about 0.25 Å is needed, which is simulated in Fig. 1a by convolving the model PDF with a Gaussian. For our 17-molecule water cells (see Sec. III) fair agreement with experiment is observed, but with a slightly stronger first-shell. The position and height of the first peak in  $g_{OO}(r)$  are sensitive to both the momentum range in the diffraction measurements and assumptions about the structure and core potentials. Discussions of these limitations can be found elsewhere, e.g.,

Refs. 17 and 33.

The total electronic density of states (DOS) provides a useful picture of the ground-state electronic structure, and, in particular, the occupied and unoccupied energy levels in these materials. A comparison of the DOS for liquid, solid, and gas-phase  $\text{H}_2\text{O}$  as calculated with ABINIT is shown in Fig. 1b. The DOS of both liquid water and ice-Ih match roughly, apart from broadening and the sharp peak at about +10 eV in ice. The resemblance between the densities of state of the two condensed systems suggests that the electronic structure is most strongly dependent on local, short-range order. The additional broadening in the liquid reflects the larger configurational disorder in amorphous structures. In contrast, the unoccupied DOS of the gas phase shows considerably more structure than either the liquid or solid phases. These results for the DOS are similar to previous work, e.g., Chen et al.<sup>15</sup>

### C. GW Self-energy

Quasi-particle self-energy effects are of crucial importance in broad-spectrum calculations of optical and x-ray spectra. DFT calculations of the ground state systematically underestimate band gaps and conduction band widths compared to experimental results, e.g., inverse photoemission. A comparison of our GW many-pole self-energies for water and ice is shown in Fig. 2. Note that the imaginary parts are quite similar and grow significantly above about 15 eV, and the real parts also differ little. This reflects the close similarity between the valence dielectric response (i.e.,  $\epsilon_2$  and  $-\text{Im}\epsilon^{-1}$ ) of water and ice, and leads to an overall stretch of the spectra by about 1 eV. The MPSE approximation to the self-energy fails to fully correct the gap in these systems, so the optical spectra that follow have been aligned to match the observed gap.

## III. ICE SPECTRA

Water has a rich phase diagram with at least 12 crystalline phases of ice, 9 of which are stable, in addition to several amorphous phases. Complicating the discussion of  $\text{H}_2\text{O}$ , ice is proton disordered, but this cannot be treated well by our approach which enforces periodic boundary conditions. Of the known, stable phases of ice, only ice-VIII has proton ordering with an anti-ferroelectric unit cell. Recent investigations of the proton ordering phase transition between ices VII and VIII found no significant difference in the Oxygen K edge NRIXS, implying that the effect of proton disorder on that spectrum is small.<sup>34</sup>

In addition to local fluctuations in the dipole moments of most phases of ice, the low-mass hydrogen atoms have a significant amount of zero-point motion on top of thermal vibrations, which is not captured by standard Born-

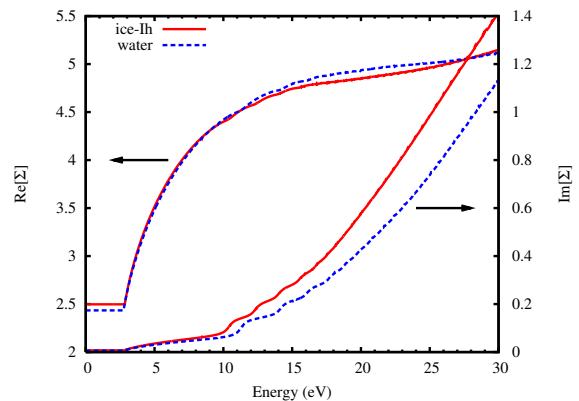


FIG. 2: (Color online) Comparison of GW self-energies for solid and liquid water as calculated with our MPSE model.<sup>27</sup> Note that these are quite similar, indicative of similar broadening and self-energy damping effects in water and ice. The quasi-particle self-energy broadening may be compared to other sources of broadening in the spectra: experimental resolutions ( $\approx 0.5$  eV), the O 1s core-hole lifetime (0.16 eV), and vibrational broadening which is yet smaller and not included.

Oppenheimer molecular dynamics. It has been shown that including zero-point motion disorder leads to a broadening of the unoccupied states in  $\text{H}_2\text{O}$  systems, improving agreement with experiment for the overall edge width.<sup>16</sup> Once again, accurate treatment of this disorder requires larger unit cells, containing 32 or 64 molecules, which are not feasible in our current implementation. Recent work has focused on capturing the quantum nature of the hydrogen movement, but such improvements are not included here.<sup>35</sup>

### A. Ice Models

For this study we have focused on two forms of ice; ice-VIII, which is stable below 273 K and pressures in the range of 2 GPa to 50 GPa, and ice-Ih, which is the common form of ice, stable under ambient pressure. Our ice-Ih model uses a 16-molecule cell determined by enforcing the experimental density and following the ice rules for hydrogen placement with an O-H bond distance and angle of 1.01 Å and  $106^\circ$  respectively. A realistic simulation of ice-Ih should have full proton disorder, but our models are based on small cells with periodic boundary conditions and thus contain artificial order. Further calculations for other ice-Ih models using larger unit cells and finite temperature configuration sampling are called for to assess the validity of our simplified model.

Ice-VIII is formed under high pressure at temperatures below the conventional freezing point of water. The pressure requirements preclude experimental techniques incompatible with diamond-anvil cells such as lower energy XAS measurements. However, NRIXS can probe the same final-state as XAS with an additional tunable parameter  $\mathbf{q}$ , the momentum transfer, and at a much

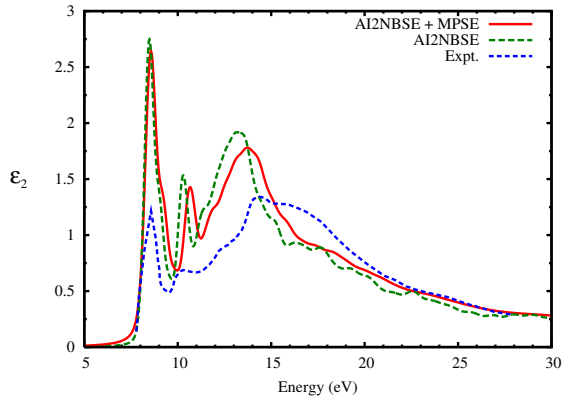


FIG. 3: (Color online) The imaginary part of the dielectric constant of ice-Ih calculated using AI2NBSE with the MPSE correction (solid red) and with a static energy shift (dashed green). For comparison an experimental measurement of ice-Ih is shown (dotted blue).<sup>37</sup> The discrepancy likely reflects a lack of disorder in our model structure (see text).

higher beam energy. The structure of ice-VIII is that of two interpenetrating cubic ice lattices resulting in a compressed second shell and higher densities than ice-Ih. The unit cell contains only 4 molecules and has anti-ferroelectric Hydrogen ordering, making it the least computationally intensive ice structure to simulate. Our ice-VIII cell uses the experimental lattice constants at a pressure of 2.4 GPa.<sup>36</sup>

### B. Ice valence spectra

For the ice-Ih spectra, the wavefunctions from ABINIT were calculated on a  $4 \times 4 \times 4$   $k$ -point mesh with 464 bands (400 conduction bands). For comparison, the structure and valence spectrum of hexagonal ice (ice-Ih) were studied previously with DFT/BSE approaches, yielding qualitative agreement with experiment.<sup>22</sup> For the valence spectrum (Fig. 3), the calculated excitonic peaks at 8 eV and 10 eV are significantly stronger than that measured. Between 10 eV and 20 eV the absorption is also too strong and too thinly peaked compared to experiment which exhibits additional broadening past 15 eV. These discrepancies are partly due to the lack of disorder in our model structure and point to the need to consider more elaborate models that can account for such disorder. The effect of the MPSE is seen as a stretch of the spectra together with energy dependent broadening. Coupling between electronic excitations and phonons is expected to provide small additional broadening, but is not included in this work.

### C. Ice core spectra

For the oxygen K edge XAS and NRIXS calculations a  $4 \times 4 \times 4$   $k$ -point mesh and 400 conduction bands were used

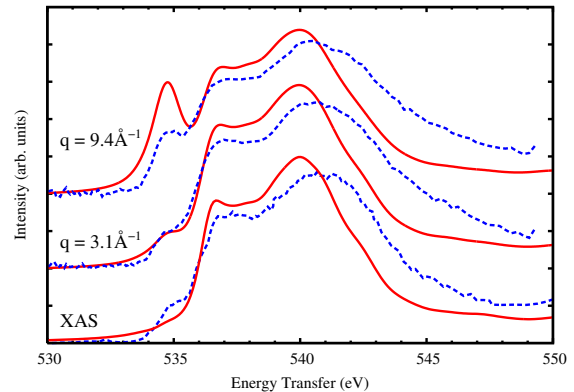


FIG. 4: The calculated momentum-transfer dependence of the oxygen K edge in ice-Ih (solid red), including the MPSE. For comparison experimental results (dashed blue) for XAS<sup>38</sup> and NRIXS<sup>34</sup> are shown.

for the BSE calculation and 900 bands for the screening. Oxygen K edge XAS and NRIXS results for ice-Ih are shown in Fig. 4. All calculated x-ray spectra have been broadened by convoluting with a Lorentzian to account for the core-hole lifetime and a Gaussian to match reported experimental broadening. Further damping is provided by the imaginary part of the self-energy (cf. Fig. 2). Results are shown averaged over orthogonal incident photon polarizations or momentum transfers for XAS and NRIXS respectively since experimental data is reported for polycrystalline samples.

Our XAS calculation matches experiment fairly well, but it has a lower pre-edge (535 eV) and is noticeably too narrow in overall width (Fig. 4). Recently the momentum dependence of the O K edge in ice has been measured using NRIXS.<sup>34</sup> The theoretical simulation of NRIXS with OCEAN differs only slightly from XAS in that the finite momentum transfer  $\mathbf{q}$  can break the dipole selection rules, allowing transitions to  $s$ -type and higher angular momentum final states. Overall the calculations yield fair agreement for the spectra, including both the relative weights and the momentum dependence of the pre-edge feature (Fig. 4). However, the balance between the  $s$ - and  $p$ -character of the pre-edge is shifted too much towards the  $s$ -type in our calculation, leading to overly strong growth of the pre-edge with increasing  $\mathbf{q}$ . Note that experiment shows little difference between  $\mathbf{q} \approx 0$  (XAS) and  $\mathbf{q} = 3.1$ .

We have also examined the momentum dependence of ice-VIII (Fig. 5) which exhibits a similar evolution with increasing  $\mathbf{q}$  as ice-Ih and good general agreement with experiment. Like ice-Ih, our calculations of the O K edge in ice-VIII are too strongly peaked in the main edge and have too little weight above about 543 eV when compared to experiment but show improvements over previous theoretical results.<sup>39</sup> Similar to ice-Ih, the calculations of ice-VIII also show excessive  $\mathbf{q}$  dependence for the pre-edge, thus suggesting either a limitation of the DFT wave functions or the need to consider thermal and quantum

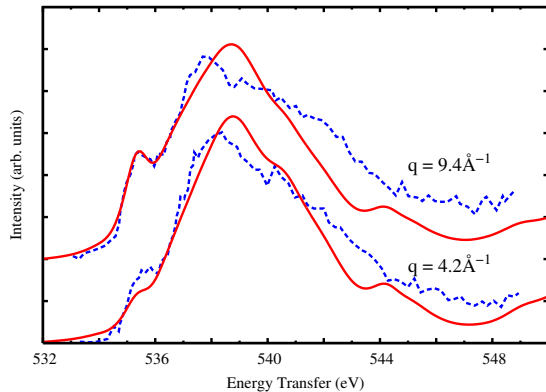


FIG. 5: (Color online) The calculated (solid red) momentum transfer dependence of the oxygen K edge in ice-VIII NRIXS compared with experiment (dashed blue)<sup>34</sup> for small ( $\mathbf{q} = 4.2 \text{ \AA}^{-1}$ ) and large ( $\mathbf{q} = 9.4 \text{ \AA}^{-1}$ ) momentum transfer. The energy of the theory has been shifted 0.9 eV higher compared to the ice-Ih and water x-ray calculations.

disorder.

#### IV. WATER: 17-MOLECULE LIQUID CELLS

##### A. Water structural model

Our calculations for optical and x-ray spectra were carried out on 17-molecule snapshots for liquid water obtained from the molecular dynamics (MD) results of Garbuio et al.<sup>23</sup> Despite the small size of these model structures, they already exhibit substantial disorder and are found to have a pair-distribution function (Fig. 1) in fairly good agreement with experiment. However, while bulk water is a disordered system with no net dipole moment, the limited cell size of our systems precludes this constraint; for our samples the moments were found to vary widely from 14 Debye to 28 Debye.

##### B. Water valence spectra

For the valence calculation a  $4 \times 4 \times 4$   $k$ -point mesh and 300 conduction bands were used, and both a static energy shift of 4.13 eV, as suggested by Garbuio et al.,<sup>23</sup> as well as the energy dependent MPSE were applied. With the static shift the positions of the initial peaks match well with experiment (Fig. 6) and in general, the agreement is excellent over the full range of the spectra. Our results for the peak positions in  $\epsilon_2$  agree qualitatively with those of Garbuio et al. but yield features that are smaller in overall magnitude. The energy dependence of our MPSE (Fig. 2) introduces a stretch in the spectrum of  $\approx 5\%$  in the range of 10 eV to 20 eV, while Garbuio et al. reported the GW energy correction to be almost constant across the low-lying conduction bands for water.

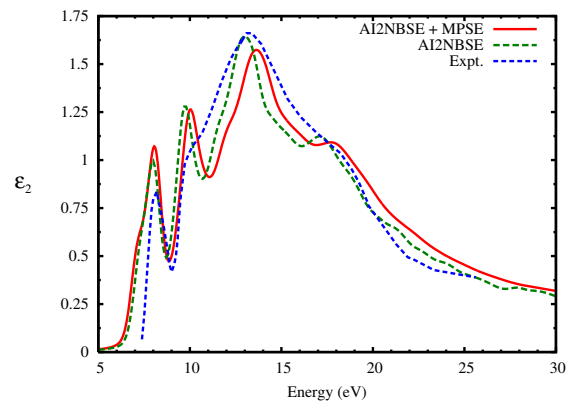


FIG. 6: (Color online) Calculated  $\epsilon_2$  spectra for a single MD snapshot with a 17-molecule water cell using the MPSE (solid red) and a static energy shift (dashed green) compared to experiment (dotted blue).<sup>40</sup>

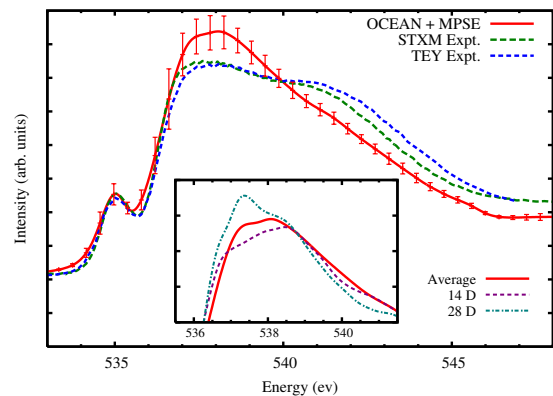


FIG. 7: (Color online) The XANES spectra for the O K edge in water. The OCEAN results, including the many-pole self-energy, are compared with recent Scanning Transmission X-ray Microscopy (STXM)<sup>41</sup> and Total Electron Yield (TEY) experiments.<sup>42</sup> The error-bars for the calculation represent the rms variation between the 8 different MD snapshots, showing reasonable similarity between the spectra from different geometries sampled by the MD despite the limited cell size. Inset: The main edge for the MD snapshots with the lowest and highest dipole moments compared to average (solid). With decreasing dipole moment the first peak intensity decreases with a slight shift to higher energies, a trend consistent with a decrease in the discrepancy with experiment as the net dipole moment approaches zero.

##### C. Water core spectra

XAS calculations were carried out for 8 of the MD snapshots using a  $4 \times 4 \times 4$   $k$ -point mesh including 300 bands for the final states and 400 conduction bands for the screening. The screened core-hole potential was found to be nearly identical for different O sites within a cell, reflecting the molecular character of liquid water. The O K-shell XAS calculation (Fig. 7) exhibits considerable variation among the different oxygen sites both

within a cell and between cells. Both the calculated and recent experimental spectra<sup>41,42</sup> exhibit a notable intensity shift and increased broadening going from ice to water, shifting spectral weight to the lower part of the spectrum from 534 eV to 538 eV. The calculated O K edge spectra is in good agreement with experiments when corrected with the MPSE, but, as for the calculated ice-Ih spectra, the main edge at about 536 eV is stronger than in experiment. The peak at 541 eV in experiment is evident in the calculation but is lacking in strength. The success of the MPSE in correcting the overall width of the near-edge is consistent with calculations using the COHSEX approximation<sup>15</sup> but in contrast to earlier work<sup>23</sup> which showed that the self-energy for water was nearly constant for their  $G^0W^0$  approximation.

We find that the unphysical dipole moments of the the small unit-cells in this study have a systematic effect on the calculated spectra (inset of Fig. 7). That is, the two main peaks of the calculated O K edge at 537 eV and 540 eV exhibit shifts in intensity and position that loosely correlate with dipole moment, i.e., the local, static electric field felt by each water monomer in the ground state. At higher values of the dipole moment the main edge features shift to lower energies, increasing discrepancy with experiment. This again points to the need for simulations with larger cells that more accurately characterize the model structure and properties.

## V. SUMMARY AND FUTURE PROSPECTIVE

Theoretical calculations have been carried out for both valence and core spectra of a number of model ice and water systems using modern GW/BSE theoretical methods. Our results suggest that accurate calculations of the spectra for these systems are quite sensitive both to the theoretical methods and details of the model structures. Nevertheless, we have shown that the improved treatment of many-body effects in the present approach yields better agreement with experiment in terms of both relative peak weights as well as overall width and feature locations compared to calculations that ignore these effects.

We find that the inclusion of an accurate quasi-particle self-energy is important to characterize the damping and self-energy shifts in the spectra. In particular we find that the stretch provided by our GW MPSE significantly improves the agreement between calculations and experiment for the ice and water systems. Our results for the valence  $\epsilon_2$  spectra for the 17-molecule water model differ somewhat from those of Garbuio et al. Theirs have somewhat larger values of  $\epsilon_2$ , while ours exhibits an extra excitonic peak. The origin of these differences is likely due to differences in the screening approximations used. In any case, our present results appear to be in reasonable agreement with recent experimental results for both the core and valence spectra of water.

Our calculated x-ray spectra for these ice and water

systems are systematically too narrow, and at present we can not account for this discrepancy. We suggest that configurational averages should be carried out for ice-Ih and ice-VIII to better understand the effects of disorder, finite temperature, and zero-point variations in structure on BSE-based spectroscopy of ice and water systems. Variation in hydrogen positioning and bonding from finite temperature and zero-point motion effects has been shown within a different theoretical approach to increase the overall width of features in the XAS of ice and water.<sup>16</sup> Additionally, convergence should be checked with respect to the size of the cells being used, especially because larger cells should allow for better control of the net dipole moment. Larger cells will become feasible with improved parallelization of our code. The oxygen K edge should be calculated for a sufficient number of MD snapshots to ensure a good representation of the physical system. Site-specific geometrical information, i.e., bond length, angles, and hydrogen bond coordination, can then be compared to contributions from individual oxygen XANES to correlate differences in local environment and calculated XAS/NRIXS.

**ACKNOWLEDGMENTS:** We thank R. Car, G. Galli, D. Prendergast, F. Gygi, O. Pulci, L. Pettersson, A. Nilsson, and M. Ljungberg for many helpful and stimulating discussions. We are especially grateful to O. Pulci for supplying the 17-molecule water cells used in this work and to L. Pettersson and A. Nilsson for making available recent experimental data. This work was supported in part by DOE Grant DE-FG03-97ER45623 and used resources of the National Energy Research Scientific Computing Center, which is supported by the Office of Science of the U.S. Department of Energy under Contract No. DE-AC02-05CH11231. One of us (JJR) also wishes to thank to acknowledge the Kavli Institute for Theoretical Physics Santa-Barbara and the Ecole Polytechnique (Palaiseau, France) for hospitality during the completion of this work.

- 
- <sup>1</sup> A. K. Soper, *Pure Appl. Chem.* **82**, 1855 (2010).
  - <sup>2</sup> M. Cavalleri, H. Ogasawara, L. Pettersson, and A. Nilsson, *Chem. Phys. Lett.* **364**, 363 (2002).
  - <sup>3</sup> S. Myneni, Y. Luo, L.-Å. Näslund, M. Cavalleri, L. Ojamäe, H. Ogasawara, A. Pelmeshnikov, P. Wernet, P. Väterlein, C. Heske, et al., *J. Phys.: Condens. Matter* **14**, L213 (2002).
  - <sup>4</sup> U. Bergmann, P. Wernet, P. Glatzel, M. Cavalleri, L. G. M. Pettersson, A. Nilsson, and S. P. Cramer, *Phys. Rev. B* **66**, 092107 (2002).
  - <sup>5</sup> P. Wernet, D. Nordlund, U. Bergmann, M. Cavalleri, M. Odelius, H. Ogasawara, L.-Å. Näslund, T. K. Hirsch, L. Ojamäe, P. Glatzel, et al., *Science* **304**, 995 (2004).
  - <sup>6</sup> D. Prendergast and G. Galli, *Phys. Rev. Lett.* **96**, 215502 (2006).
  - <sup>7</sup> B. Hetényi, F. D. Angelis, P. Giannozzi, and R. Car, *J. Chem. Phys.* **120**, 8632 (2004).
  - <sup>8</sup> G. Brancato, N. Rega, and V. Barone, *Phys. Rev. Lett.* **100**, 107401 (2008).
  - <sup>9</sup> J. D. Smith, C. D. Cappa, K. R. Wilson, B. M. Messer, R. C. Cohen, and R. J. Saykally, *Science* **306**, 851 (2004).
  - <sup>10</sup> A. Nilsson, P. Wernet, D. Nordlund, U. Bergmann, M. Cavalleri, M. Odelius, H. Ogasawara, L.-Å. Näslund, T. K. Hirsch, L. Ojamäe, et al., *Science* **308**, 793 (2005).
  - <sup>11</sup> J. D. Smith, C. D. Cappa, B. M. Messer, R. C. Cohen, and R. J. Saykally, *Science* **308**, 793 (2005).
  - <sup>12</sup> M. Cavalleri, M. Odelius, D. Nordlund, A. Nilsson, and L. G. M. Pettersson, *Phys. Chem. Chem. Phys.* **7**, 2854 (2005).
  - <sup>13</sup> M. Odelius, M. Cavalleri, A. Nilsson, and L. G. M. Pettersson, *Phys. Rev. B* **73**, 024205 (2006).
  - <sup>14</sup> M. Iannuzzi, *J. Chem. Phys.* **128**, 204506 (2008).
  - <sup>15</sup> W. Chen, X. Wu, and R. Car, *Phys. Rev. Lett.* **105**, 017802 (2010).
  - <sup>16</sup> M. Leetmaa, M. Ljungberg, A. Lyubartsev, A. Nilsson, and L. Pettersson, *J. Electron Spectrosc. Rel. Phenom.* **177**, 135 (2010).
  - <sup>17</sup> K. T. Wikfeldt, M. Leetmaa, M. P. Ljungberg, A. Nilsson, and L. G. M. Pettersson, *J. Phys. Chem. B* **113**, 6246 (2009).
  - <sup>18</sup> T. T. Fister, K. P. Nagle, F. D. Vila, G. T. Seidler, C. Hamner, J. O. Cross, and J. J. Rehr, *Phys. Rev. B* **79**, 174117 (2009).
  - <sup>19</sup> G. Onida, L. Reining, and A. Rubio, *Rev. Mod. Phys.* **74**, 601 (2002).
  - <sup>20</sup> H. M. Lawler, J. J. Rehr, F. Vila, S. D. Dalosto, E. L. Shirley, and Z. H. Levine, *Phys. Rev. B* **78**, 205108 (2008).
  - <sup>21</sup> J. Vinson, J. J. Rehr, J. J. Kas, and E. L. Shirley, *Phys. Rev. B* **83**, 115106 (2011).
  - <sup>22</sup> P. H. Hahn, W. G. Schmidt, K. Seino, M. Preuss, F. Bechstedt, and J. Bernholc, *Phys. Rev. Lett.* **94**, 037404 (2005).
  - <sup>23</sup> V. Garbuio, M. Cascella, L. Reining, R. DelSole, and O. Pulci, *Phys. Rev. Lett.* **97**, 137402 (2006).
  - <sup>24</sup> X. Gonze, B. Amadon, P.-M. Anglade, J.-M. Beuken, F. Bottin, P. Boulanger, F. Bruneval, D. Caliste, R. Caracas, M. Cote, et al., *Computer Phys. Commun.* **180**, 2582 (2009).
  - <sup>25</sup> X. Gonze, G.-M. Rignanese, M. Verstraete, J.-M. Beuken, Y. Pouillon, R. Caracas, F. Jollet, M. Torrent, G. Zerah, M. Mikami, et al., *Zeit. Kristallogr.* **220**, 558 (2005).
  - <sup>26</sup> J. P. Perdew and Y. Wang, *Phys. Rev. B* **45**, 13244 (1992).
  - <sup>27</sup> J. J. Kas, A. P. Sorini, M. P. Prange, L. W. Cambell, J. A. Soininen, and J. J. Rehr, *Phys. Rev. B* **76**, 195116 (2007).
  - <sup>28</sup> P. E. Blöchl, *Phys. Rev. B* **50**, 17953 (1994).
  - <sup>29</sup> E. L. Shirley, *Ultramicroscopy* **106**, 986 (2006).
  - <sup>30</sup> J. A. Soininen and E. L. Shirley, *Phys. Rev. B* **64**, 165112 (2001).
  - <sup>31</sup> S. Tinte and E. L. Shirley, *J. Phys.: Condens. Matter* **20**, 365221 (2008).
  - <sup>32</sup> S. A. Rice and M. G. Sceats, *J. Phys. Chem.* **85**, 1108 (1981).
  - <sup>33</sup> A. K. Soper, *J. Phys.: Condens. Matter* **19**, 335206 (2007).
  - <sup>34</sup> T. Pyllkkänen, V. M. Giordano, J.-C. Chervin, A. Sakko, M. Hakala, J. A. Soininen, K. Hämäläinen, G. Monaco, and S. Huotari, *J. Phys. Chem. B* **114**, 3804 (2010).
  - <sup>35</sup> J. A. Morrone and R. Car, *Phys. Rev. Lett.* **101**, 017801 (2008).
  - <sup>36</sup> W. F. Kuhs, J. L. Finney, C. Vettier, and D. V. Bliss, *J. Chem. Phys.* **81**, 3612 (1984).
  - <sup>37</sup> M. Seki, K. Kobayashi, and J. Nakahara, *J. Phys. Soc. Japan* **50**, 2643 (1981).
  - <sup>38</sup> J. S. Tse, D. M. Shaw, D. D. Klug, S. Patchkovskii, G. Vankó, G. Monaco, and M. Krisch, *Phys. Rev. Lett.* **100**, 095502 (2008).
  - <sup>39</sup> D. M. Shaw and J. S. Tse, *J. Phys.: Condens. Matter* **19**, 425211 (2007).
  - <sup>40</sup> J. J. M. Heller, R. N. Hamm, R. D. Birkhoff, and L. R. Painter, *J. Chem. Phys.* **60**, 3483 (1974).
  - <sup>41</sup> A. Nilsson, D. Nordlund, I. Waluyo, N. Huang, H. Ogasawara, S. Kaya, U. Bergmann, L.-Å. Näslund, H. Öström, P. Wernet, et al., *J. Electron Spectrosc. Rel. Phenom.* **177**, 99 (2010).
  - <sup>42</sup> C. D. Cappa, J. D. Smith, K. R. Wilson, and R. J. Saykally, *J. Phys.: Condens. Matter* **20**, 205105 (2008).